Eurasian Journal of Physics and Functional Materials

Volume 9 | Number 3

Article 8

Pages: 1 - 15

2025

Organic thin-film transistors based on thin films of polymer and nanocomposite materials

Salikhov Renat
Institute of Physics and Technology, Ufa University of Science and Technology, Russian Federation

Ostaltsova Anastasiya
Institute of Physics and Technology, Ufa University of Science and Technology, Russian Federation

Salikhov Timur
Institute of Physics and Technology, Ufa University of Science and Technology, Russian Federation.

Balapanov Malik
Institute of Physics and Technology, Ufa University of Science and Technology, Russian Federation., balapanovmk@mail.ru

Kubenova Marzhan
Institute of Physics and Technology, L.N. Gumilyov Eurasian National University, 010008 Astana, Kazakhstan Republic.

Organic thin-film transistors based on thin films of polymer and nanocomposite materials

Authors

Salikhov Renat, Ostaltsova Anastasiya, Salikhov Timur, Balapanov Malik, Kubenova Marzhan, and Aida B. Akberdiyeva

REVIEW

Organic Thin-film Transistors Based on Thin Films of Polymer and Nanocomposite Materials

Renat B. Salikhov [a], Anastasiya D. Ostaltsova [a], Timur R. Salikhov [a], Malik Kh. Balapanov [a,*], Marzhan M. Kubenova [b], Aida B. Akberdiyeva [b]

[a] Institute of Physics and Technology, Ufa University of Science and Technology, Russian Federation
[b] Institute of Physics and Technology, L.N. Gumilyov Eurasian National University, Astana, Kazakhstan

Abstract

Thin-film organic field-effect transistors have emerged as a promising technology for flexible and low-cost electronic devices. This review examines recent advances in the development of OFTs based on various organic and nanocomposite materials, including carbon nanotubes, epoxy blends, graphene oxide, chitosan succinamide, polyarylenephthalide, fullerene derivatives, and poly(3-hexylthiophene-2, 5-diyl). The electrical properties, charge carrier mobility, and surface morphology of these materials are analyzed, highlighting their potential applications in sensors, flexible electronics, and biomedical devices. The review also discusses challenges and future directions in this field, emphasizing the need for improved fabrication methods and material optimization to enhance device performance and scalability.

Keywords: Transistors, Charge carrier mobility, Thin films, Current-voltage characteristics

1. Introduction

Organic field-effect transistors (OFETs) have attracted significant attention since their invention in 1986 due to their unique properties, such as environmental friendliness, flexibility, and lightness [1]. These attributes have led to their application in electronic circuits and various sensors, including chemical, biological, and temperature sensors [2]. The biocompatibility and low-cost nature of OFETs based on organic semiconductors (OSCs) make them particularly promising for environmental monitoring and medical diagnostics [3,4]. Substantial progress has been made in recent years in developing gas sensors for detecting NH_3, NO_2, and H_2S [5]; however, challenges with stability and reproducibility persist [6—8]. Consequently, research into charge transfer mechanisms [9—11] and the development of new polymers [12] remains highly relevant.

Thin-film organic field-effect transistors (TFOFETs) are of great interest for flexible electronics, sensors, and low-cost electronic devices due to their compatibility with large-area, low-temperature processing techniques [13—15]. A key advantage over traditional silicon-based devices is their outstanding mechanical flexibility, which is crucial for applications in wearable electronics and biomedical sensors [16]. This flexibility, often characterized by a high elastic limit and low bending modulus, allows these devices to conform to irregular surfaces, such as human skin, without structural failure. The mechanical properties of the constituent materials, including polymers and carbon nanostructures, are therefore a critical area of investigation, as referenced in studies on these composites [19,20].

As key components in electronics, transistors are vital for controlling electrical signals. Organic field-effect transistors offer a viable alternative to silicon-based devices in applications where mechanical flexibility and low manufacturing costs are essential [17]. The performance of OFETs is largely determined by the properties of the organic semiconductor materials

Received 9 June 2025; revised 16 September 2025; accepted 16 September 2025.
Available online 7 October 2025

* Corresponding author at: Zaki Validi Str. 32, 450076, Ufa City, Russian Federation.
E-mail address: BalapanovMK@mail.ru (M.Kh. Balapanov).

https://doi.org/10.69912/2616-8537.1258

used. Carbon nanostructures like carbon nanotubes (CNTs) and graphene oxide are among the most promising materials due to their high electrical conductivity, mechanical strength, and chemical stability [18]. These materials are often incorporated into polymer matrices to form nanocomposites that synergize the benefits of both components [19]. For instance, nanocomposites based on chitosan succinamide (SCTS) and polyarylenephthalide (PAP) demonstrated excellent electrical properties and biocompatibility, making them suitable for biomedical sensors [20].

Studies have shown that incorporating nanofillers into polymer matrices enhances device performance. For example, single-walled carbon nanotubes (SWCNTs) in a polyarylenephthalide matrix significantly increased charge carrier mobility to values up to 0.071 $cm^2/V \cdot s$ [21]. Similarly, the addition of graphene oxide (GO) into a chitosan succinamide matrix was shown to improve electron transport rates and effective surface area, leading to enhanced performance in electrochemical sensors [22].

The fabrication of OFETs typically involves depositing thin films of organic semiconductors onto flexible substrates like plastic or glass, followed by the deposition of gate, source, and drain electrodes. Techniques such as spin-coating and thermal evaporation are critical for producing uniform thin films with controlled morphology, which is essential for high device performance [23].

Despite considerable progress, several challenges remain. These include improving material stability, enhancing charge carrier mobility, and achieving better control over film morphology and fabrication processes [24]. Furthermore, the integration of OFETs into practical applications requires further research into scalability and cost-effectiveness [25]. Carbon nanotubes, despite their excellent properties [26–28], suffer from electrical instability [29,30] and photosensitivity [31]. While passivation methods have been explored [32,33], they have limitations [34,35], necessitating new approaches such as the use of a dual-gate architecture [36,37]. One study investigated the electrical and optical stability of CNT-based thin-film transistors prepared by a liquid-based method, demonstrating the potential of dual-gate designs to improve stability and elucidating the underlying photoresponse mechanisms [38]. CNT transistors are considered promising for flexible and transparent electronics due to their stability under low-light conditions [39,40].

Fabricating OFETs with CNTs requires optimized deposition methods. Traditional approaches like CVD and solution processing have limitations [41,42]. Dry deposition from an aerosol reactor at room temperature presents an alternative that preserves CNT properties and is compatible with flexible substrates [43–45]. Key issues such as hysteresis and the on/off ratio have been addressed by passivation methods, for example, using ALD Al_2O_3 [46,47].

Novel hybrid molecules based on fullerene C60 and strained polycyclic hydrocarbons were synthesized via the Bingel–Hirsch reaction [48–50]. Organic field-effect transistors fabricated from thin films of these fullerene C60 adducts were reported. Another study described OFETs using 1-(4-aryl-1,2,3-triazol-1-yl)-2-butylfullerene as the semiconductor layer [51]. Atomic force microscopy studies confirmed that thin films of triazolylfullerenes with 3-thienyl and 2-naphthyl groups exhibited more uniform surfaces with lower roughness.

This review provides an overview of recent advances in thin-film OFETs, focusing on carbon nanomaterials and polymer composites. It discusses electrical properties, charge carrier mobility, and surface morphology of these materials, as well as their potential applications in flexible electronics and sensors. Finally, it addresses ongoing challenges and future directions aimed at realizing the full potential of OFETs in practical applications.

2. Organic materials and nanocomposites for OFET, as well as their current-voltage characteristics

Organic materials and nanocomposites play a key role in the development of thin-film field-effect transistors, providing flexibility, low manufacturing cost, and tunability of electronic properties. Organic materials, including conjugated polymers and low-molecular compounds (e.g., pentacene, thiophene derivatives), unlike classical inorganic semiconductors, have high solubility. This property allows the use of printing and solution deposition methods to form thin-film structures. To improve the performance of OFETs, including charge carrier mobility and resistance to degradation, nanocomposites based on organic matrices with the inclusion of carbon nanotubes, graphene, or inorganic nanoparticles are actively studied. Such hybrid systems combine the advantages of organic and inorganic components, providing high conductivity, mechanical strength, and stability, making them promising for applications in flexible electronics, sensors, and wearable devices.

The work [7] presents a method for creating highly efficient field-effect transistors using dry random networks of single-walled carbon nanotubes (SWCNTs) deposited at room temperature. The synthesis process involved transporting furnace-grown nanotubes with a carbon monoxide flow followed by deposition in an

electrostatic precipitator (EP) without heating the substrate. The EP design included a cylindrical chamber with a horizontally located metal electrode for placing the substrate [52].

The electrodes (drain and source) were formed by electron-beam evaporation (IM9912 setup) with the creation of a multilayer Ti (20 nm)/Au (100 nm) structure using standard photolithographic technology with subsequent lift-off. The geometric parameters of the channels varied in the following ranges: length L from 2 to 50 μm, width W from 10 to 200 μm. The configuration of the CNTN transistor is shown in Fig. 1a.

Additionally, a passivation layer of Al_2O_3 was applied to the finished structure using atomic layer deposition (ALD). The Kapton 200 HN polymer with a thickness of 50.8 μm, which has high flexibility and mechanical strength, was used as a substrate for the top-gate architecture. After deposition of SWCNTs on the polymer substrate, electrodes (Ti 20 nm/Au 50 nm) were formed using electron beam evaporation and standard photolithography. The gate dielectric (Al_2O_3 100 nm) was created using the ALD method, and the final stage was the formation of the top gate electrode (Al 50 nm) using a similar manufacturing technology. The schematic of this structure is shown in Fig. 1b.

The current-voltage characteristics of the transistors from Ref. [7] are shown in Fig. 2. Although their parameters exceeded those of most organic thin-film transistors (TFTs), the study presented in Ref. [7] was aimed at further increasing the effective carrier mobility in top-gate TFT structures by optimizing their architecture. The findings of that work open up new prospects for creating flexible electronics based on single-layer carbon nanotubes. Fig. 2 presents the output characteristics of the thin-film transistor at different gate voltages. The **main plot** shows the full range of measured, illustrating the device's behavior from the linear regime at low to the saturation regime at higher, where the current plateaus. The family of curves, each taken at a specific gate voltage, demonstrates effective field-effect modulation of the channel conductance. The **inset** provides a magnified view of the low-bias, linear operating region. This detailed view is crucial for accurately estimating key parameters such as the contact resistance and the intrinsic channel resistance, which can be obscured in the full-scale plot. The **dashed red line** highlights the specific trajectory used to extract the device's on-state resistance or, conversely, to calculate the conductance at a given gate bias. It effectively guides the reader's eye to the slope from which this important parameter is derived.

Organic thin-film transistors (OTFTs) based on poly (3-hexylthiophene-2,5-diyl) (P3HT) with an additional intermediate layer of pure graphene oxide were fabricated and characterized [8]. In contrast to studies that utilized chemically modified GO or reduced graphene oxide (RGO) for interface modification [X, Y], the authors of [8] employed unmodified material.

The design of the modified devices (Fig. 3) is similar to standard OTFTs except for the presence of an intermediate GO layer. As can be seen from Fig. 3, the P3HT/GO layer was located not only in the channel region, but also partially overlapped the electrodes. This solution, similar to that used in standard devices, was aimed at increasing the contact area between the gold electrodes (Au) and the P3HT/GO composite [53].

The manufacturing process of M-OTFT (modified OTFT) practically repeated the standard method, supplemented by the operation of applying a GO interlayer under the P3HT layer. For the production of S-OTFT (standard OTFT), silicon substrates with thermally grown oxide with a diameter of 100 mm were used.

In Fig. 4, the transfer characteristic of the S-OTFT at $V_{DS} = -5$ V is shown as a solid blue line, and the extrapolation line is shown in red. The threshold voltage for this device was 26.09 V. For the M-OTFT, the transfer characteristic at the same drain voltage is shown as a dotted line, with a similar red extrapolation curve. In this case, the threshold voltage was 47.24 V, which is significantly higher than the standard device.

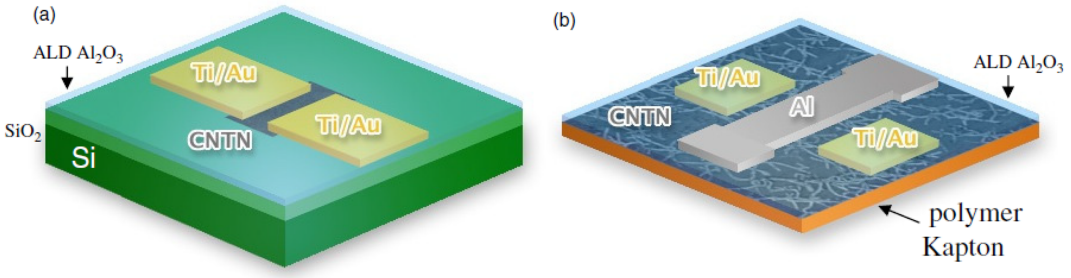

Fig. 1. Schematics of typical structures of CNTN field-effect transistors with bottom gate (a) and top gate (b) [7].

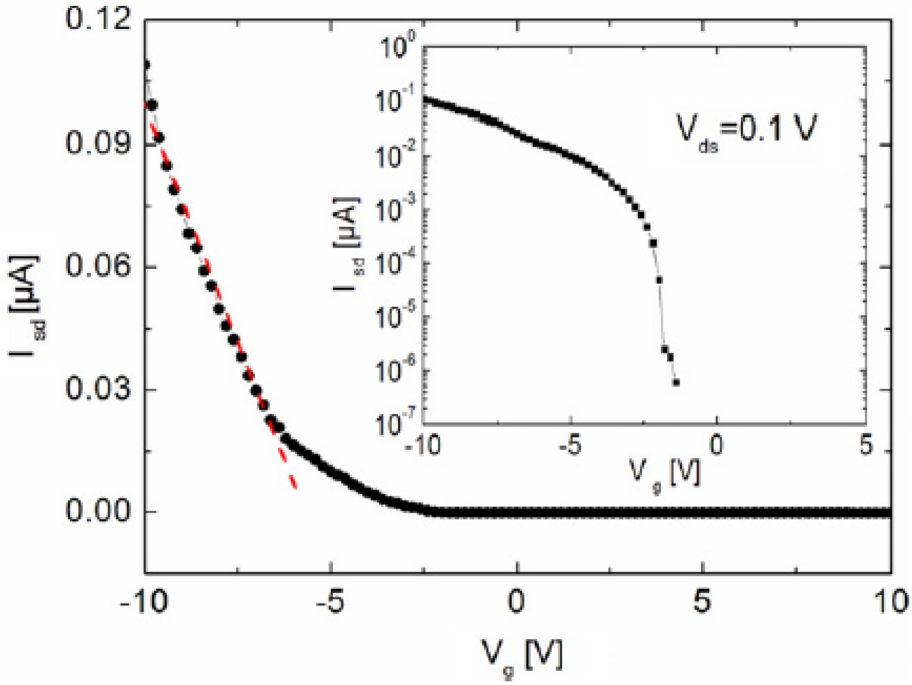

Fig. 2. I_{sd}—V_g characteristics on a polymer substrate of a typical top-gate CNTN FET [7].

Such a high threshold voltage makes the modified structure unsuitable for use in low-voltage electronics [8].

In Ref. [13], the field-effect transistor samples were fabricated using composite materials made of polyarylenephthalide (PAP) with added graphene oxide (GO) and single-walled carbon nanotubes (SWCNT). Glass plates coated with indium tin oxide (ITO) served as a substrate, acting as a gate [13] (Fig. 5).

Before depositing the dielectric layers, the substrates were heat-treated in an oven at 350 °C. 300 nm thick AlOx dielectric films were formed by spin-coating (2000 rpm, 30 s) followed by annealing at 350 °C for 1 h. At the final stage, two aluminum electrodes (drain and source), 500 nm thick each, were placed on top of the dielectric layer.

An experimental study of the volt-ampere characteristics of field-effect transistors (Fig. 6) was carried out using a common-source circuit under standard laboratory conditions (temperature 20 ± 2 °C, atmospheric pressure) [13]. The data obtained indicate n-type conductivity of the studied nanocomposite films, which is confirmed by the characteristic dependence of the output current on the positive bias on the gate.

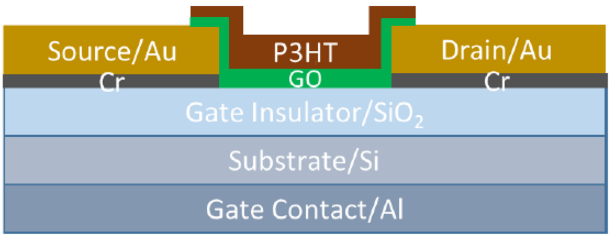

Fig. 3. Schematic structure of P3HT-based M-OTFT [8].

It should be noted that pure PAP films without GO and SWCNT additives have a conductivity several orders of magnitude lower, which excludes the possibility of observing the transistor effect in such structures.

In Ref. [14], new thin-film composite structures based on the polyelectrolyte complex chitosan-succinamide chitosan (PEC) were developed and studied. Carbon nanomaterials of various morphologies were used as modifying fillers: (Carboblack C (CB) and Carbopack (CP)). Experimental samples of field-effect transistors (Fig. 7) were made of the following composites: PEC-CarboblackC, PEC-Carbopack, PEC-GO and PEC-SWCNT.

Transistors with a transport layer made of nanocomposite materials based on PEC, CNT and GO were manufactured and their characteristics were measured (Fig. 8) [14].

Field-effect transistors were fabricated based on nanofibrous carbon (multi-walled carbon nanotubes, MWCNTs) [17]. The transistor (Fig. 9) was fabricated on a glass substrate, with a ready-made ITO film as a gate contact. The gate dielectric was made in the form of a thin film of aluminum oxide with a thickness of 390 nm by centrifugation from a solution at 1900 rpm

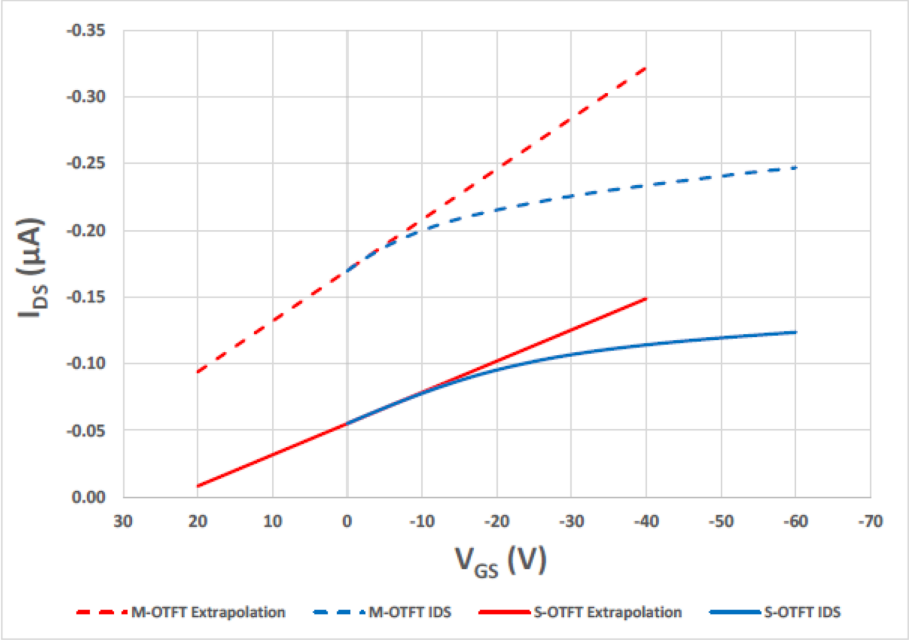

Fig. 4. Transfer and output characteristics of OFETs based on hybrid (solid lines) and separate (dashed lines) active layers [8].

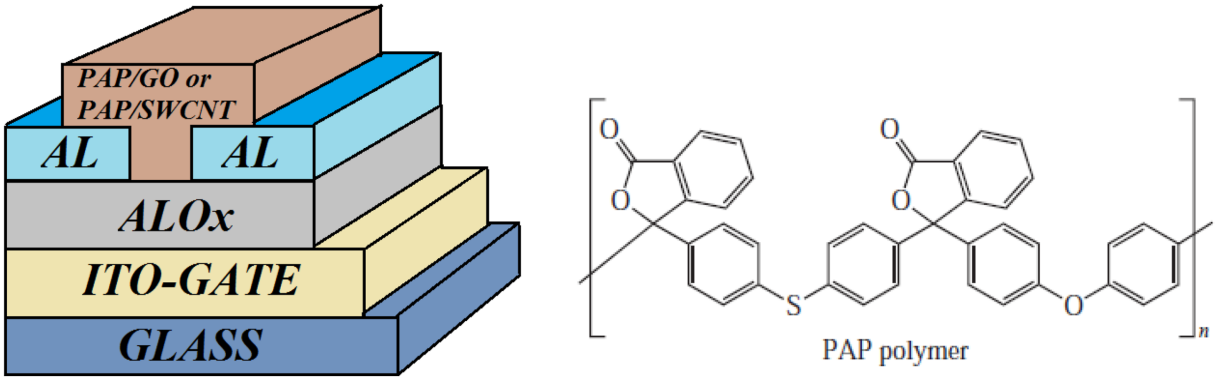

Fig. 5. The structure of the experimental field-effect transistor and PAP polymer [13].

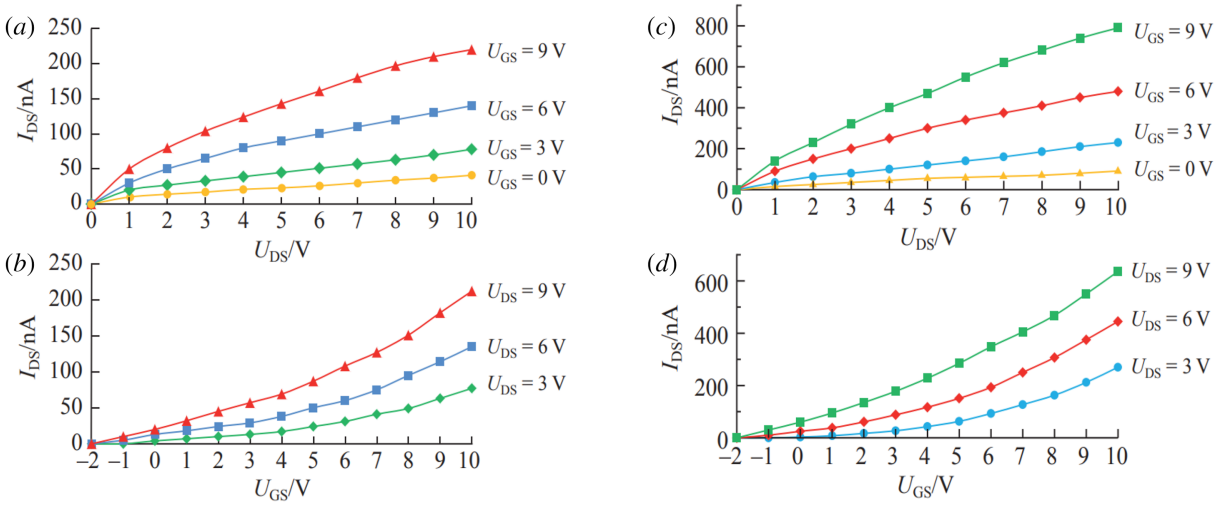

Fig. 6. Output (a) and (b) transfer characteristics of a field-effect transistor with an active layer of PAP/GO and output (c) and (d) of PAP/SWCNT [13].

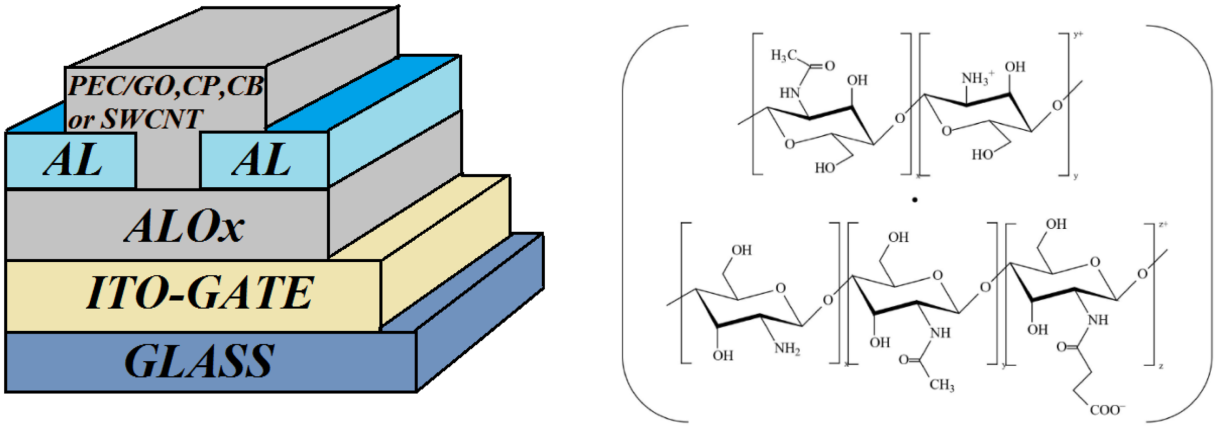

Fig. 7. Structure of the fabricated field-effect transistor and the structure of PEC based on chitosan (polycation) and chitosan succinate (polyanion) [14].

and annealing in an oven for 130 min at a temperature of 320 °C. The aluminum oxide solution was prepared as described in Refs. [54,55]. Drain-source contacts were made of aluminum foil with a thickness of 300 nm and deposited on top of the dielectric.

The current-voltage characteristics of organic field-effect transistors (Fig. 10) were studied at room temperature in an air environment. Analysis of the obtained dependencies shows that with a positive gate voltage, the current increases in these types of transistors, which indicates the electronic nature of conductivity in the transport channel.

A feature of the characteristics is their nonlinear nature, as well as the almost complete absence of saturation sections on the output current-voltage dependencies of the devices under study. The absence of saturation on the output characteristics may be due to the presence of leakage currents [17].

In Ref. [18], a thin-film transistor based on carbon nanotubes in an epoxy matrix (CNT-Epoxy) was developed. Glass with a conductive coating of indium tin oxide (ITO) was used as a substrate. The 100 nm thick gate dielectric layer was formed from an AlO_X solution. The contact pads were made of aluminum. The structure of the resulting transistor is shown in Fig. 11 [18]. A feature of this development is the

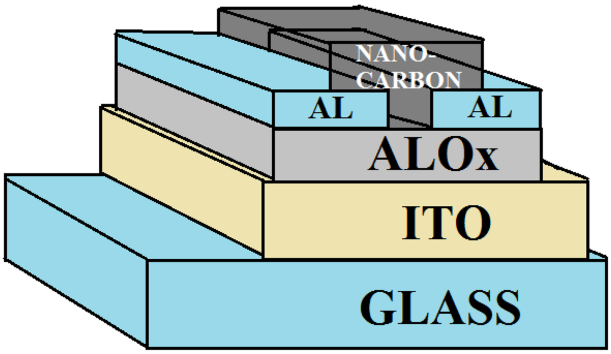

Fig. 9. Structure of the fabricated field-effect transistor [17].

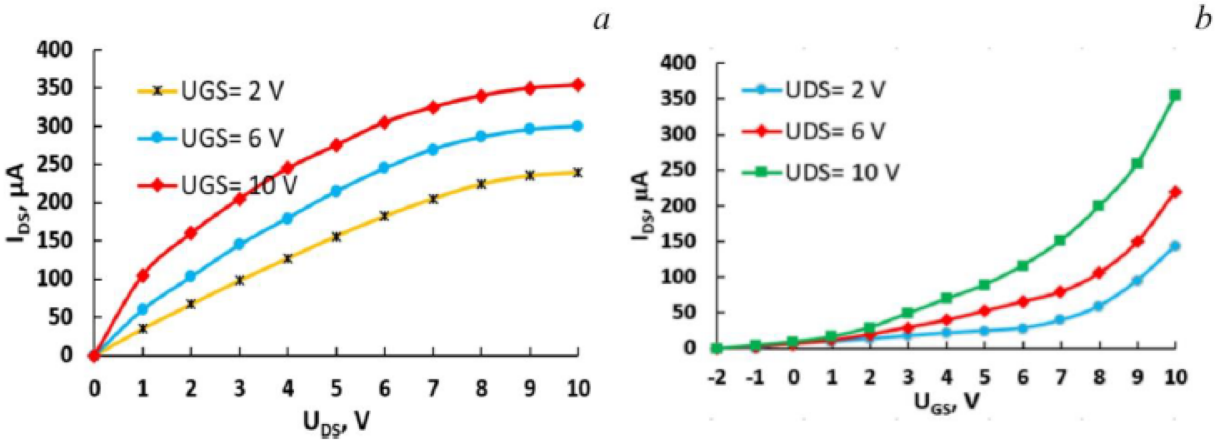

Fig. 8. Output (a) and transfer (b) characteristics of a field-effect transistor with an active layer of PEC-SWCNT-GO (synergism effect) [14].

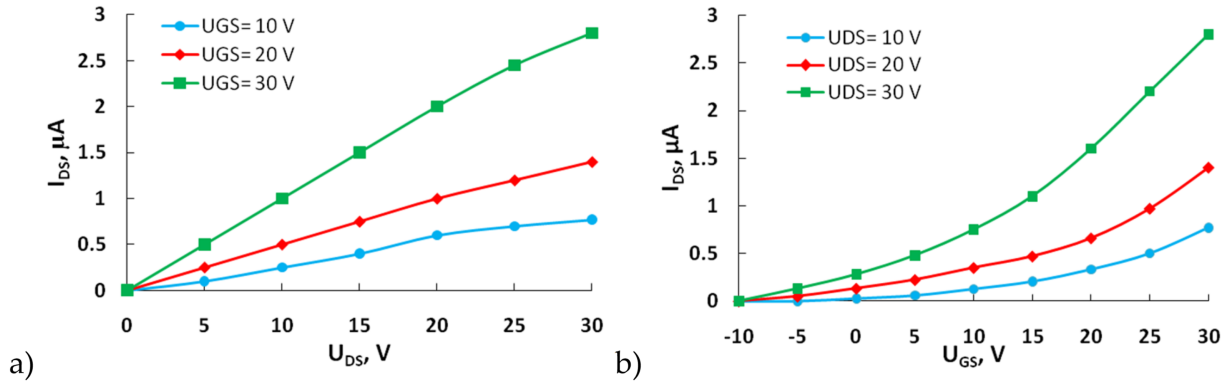

Fig. 10. Current-voltage characteristics of OFET with a transport layer made of nanocarbon (Nano-S): Output (a) transfer current-voltage characteristics of a transistor (b) [17].

ability to adjust the conductivity by changing the concentration of epoxy resin in the composite. In this case, the mass fraction of carbon nanotubes in the mixture was ≈0.3 %. Such thin-film transistors are promising for use in the following areas: sensor devices, "smart" electronic systems, where the following are critical: energy efficiency, small dimensions, design flexibility.

The current-voltage characteristics of the obtained transistors [18] are shown in the Fig. 12.

The work [51] reports the fabrication of organic field-effect transistors with triazolylfullerenes as organic semiconductors (Fig. 13). The target triazolylfullerenes 2–6 were formed in 75–90 % yield; the details of the synthesis and characterization can be found in Ref. [56].

The current-voltage characteristics of the OFETs (Fig. 14) were measured at room temperature under ambient conditions. With a positive gate voltage, the current increases for all types of transistors, which corresponds to the electron type of conductivity of the OFETs transport channel. The dependencies are nonlinear, and there are no saturation regions on the output characteristics of the devices. The absence of saturation regions on the output characteristics may be due to the presence of leakage currents [51].

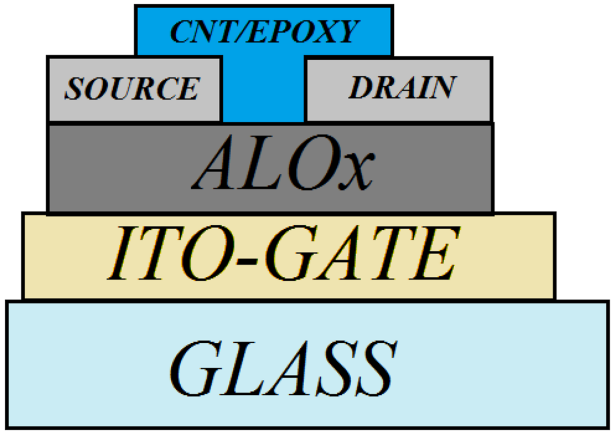

Fig. 11. Structure of a thin film transistor based on an epoxy mixture of CNTs [18].

2.1. Conclusions and future perspectives

In conclusion, there is no single "best" type of organic semiconductor for OFETs; the optimal choice is a trade-off dictated by the application:

For high-performance, flexible electronics where cost is a secondary concern, CNT-based OFETs (especially with passivation and advanced deposition) are currently the most promising, as evidenced by Ref. [7].

For ultra-low-cost, large-area applications like disposable sensors or macro-electronics, polymer-based OFETs (e.g., P3HT) offer the best pathway due to their superior processability.

Nanocomposites represent a powerful strategy for engineering material properties to achieve a specific balance of electrical, mechanical, and chemical performance, making them ideal for specialized sensor and interface applications [13,14].

Small molecules remain an important area of fundamental research for exploring charge transport mechanisms and achieving peak performance in controlled environments.

3. AFM and SEM studies of transport layers of organic transistors

The study of organic field-effect transistors is usually accompanied by the investigation of the surface morphology of the transport layers of these transistors. A typical scanning electron microscopy (SEM) image of the carbon nanotube net (CNTN) synthesized at 800 °C and deposited at room temperature on a Si/

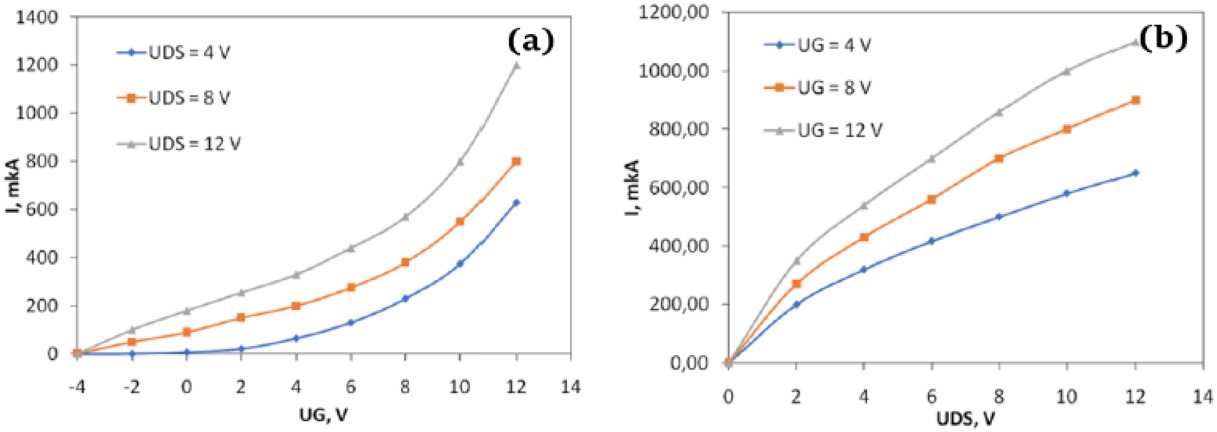

Fig. 12. Output (a) and transfer (b) characteristics of an epoxy blended CNT transistor [18].

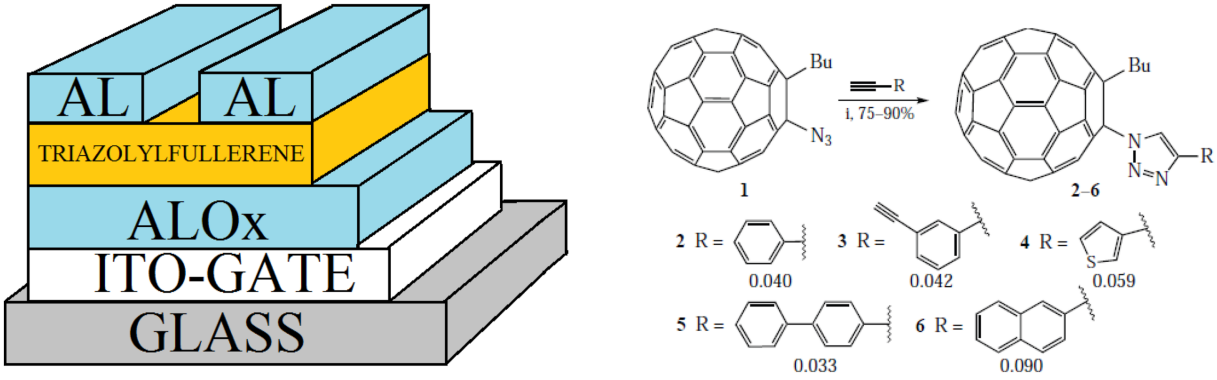

Fig. 13. Structure of the experimental field-effect transistor based on triazolylfullerenes and types of triazolylfullerenes [51,56].

SiO_2 substrate [7] is shown in Fig. 15. HWG (hot-wire generator) is a method for synthesizing single-walled carbon nanofibers (SWCNTs) with a floating catalyst. The HWG-synthesized SWCNTs with an average individual CNT length of 1 μm and an average diameter of 1 nm were used to fabricate transistors on a polymer substrate [57]. To measure the performance of the deposited CNTNs, both bottom-gate and top-gate FET structures were fabricated.

The conducted studies of the surface morphology of the P3HT layer deposited on the SiO_2 substrate [8] revealed a pronounced granular structure (Fig. 16a). Analysis of the topographic image by atomic force microscopy showed that the grain size varies in the range of 80–200 nm. The root-mean-square surface roughness is ~2 nm, which corresponds to a grain height of about 4 nm. With a layer thickness of approximately 58 nm (less than the transverse size of the grains), it can

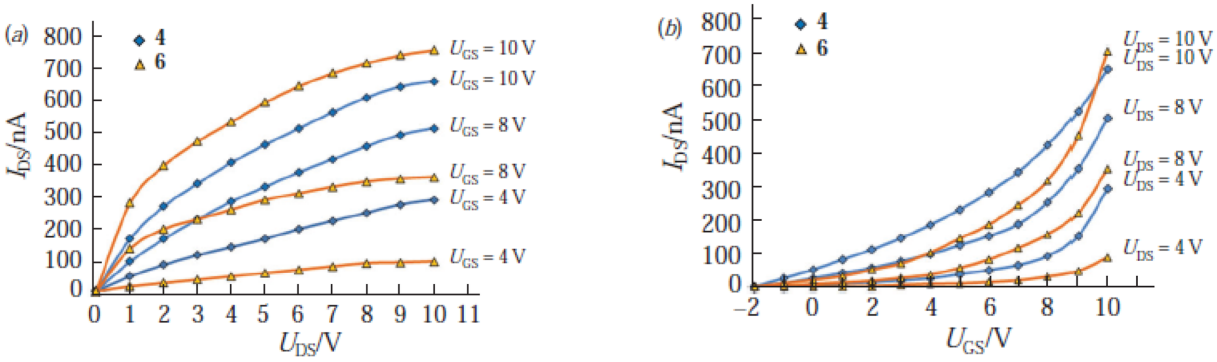

Fig. 14. Output and transfer characteristics of OFETs based on triazolylfullerenes 4 and 6 [51].

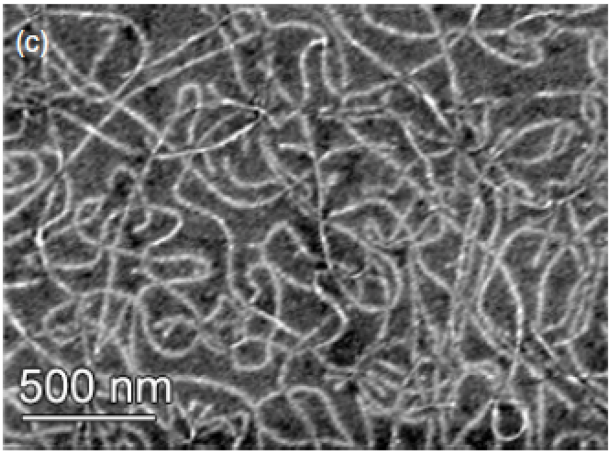

Fig. 15. SEM image of a CNTN on a Si/SiO2 substrate at room temperature using the ESP [7].

be assumed that the grain structure is the dominant morphological element in S-OTFT structures.

The phase image of the P3HT layer on SiO_2 (Fig. 16b) in the first approximation repeats the topographic features of the surface. However, characteristic wave-like irregularities with a transverse size of 30–60 nm are additionally observed, which is confirmed by AFM measurements. According to literature data [58–60], such structures may reflect the lamellar packing of P3HT macromolecules on the surface.

It is noteworthy that the morphology of P3HT deposited on the GO layer (Fig. 16c) demonstrates a fundamentally different organization. In this case, the formation of significantly larger grains is observed, forming continuous ribbon structures.

The morphology of the surfaces of the films was also studied. AFM images (Fig. 17) were obtained using Nanoeducator II [13]. The PAP/GO surface showed high peaks, which are shown in white, while the PAP/SWCNT surface had a “softer” structure.

Scanning electron microscopy (Fig. 18) allowed us to visualize the distribution of carbon (yellow) over the film surface. The analysis revealed significant changes in morphology when moving from pure PEC to its composite forms with single-walled carbon nanotubes or graphene oxide. Key morphological features: pure

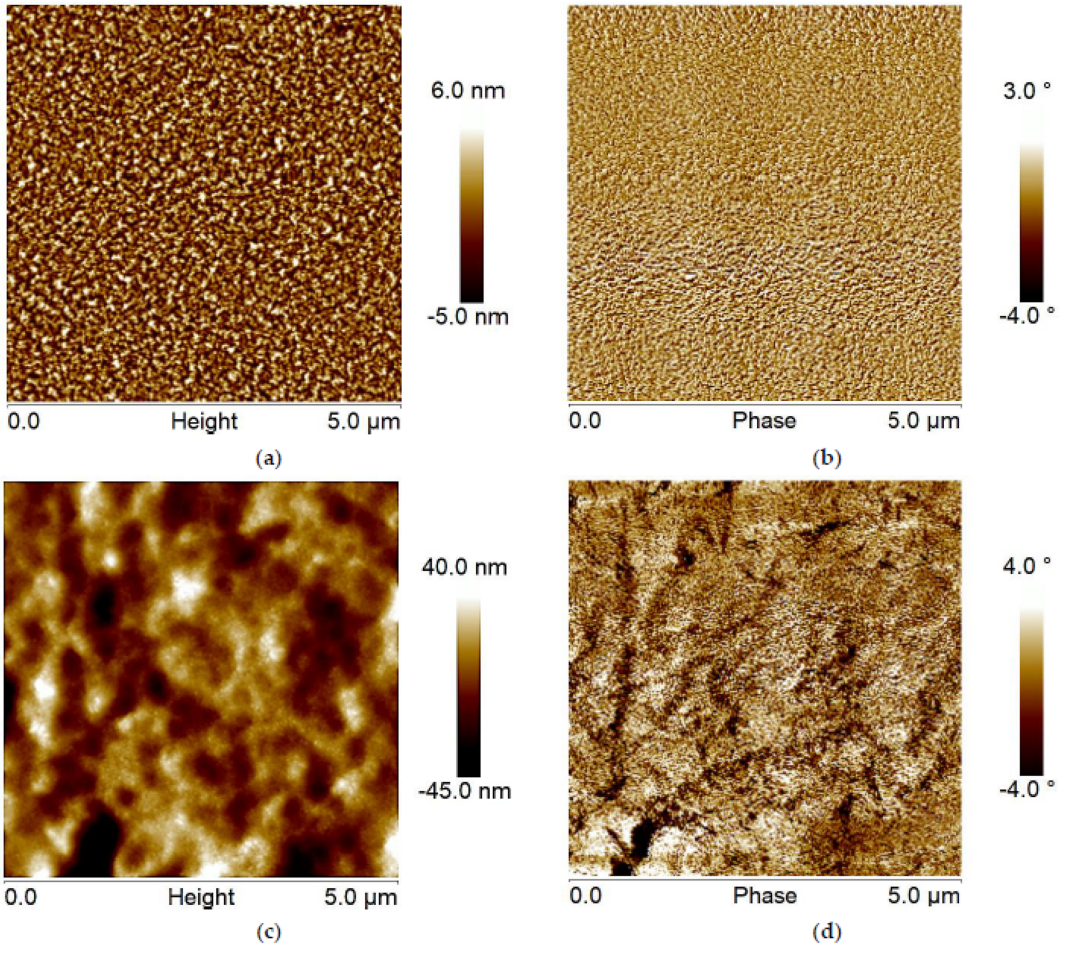

Fig. 16. Photoresponce kinetics of current through polyindole films obtained at different spin-coating rates. Voltage between electrodes U = 10 V [8].

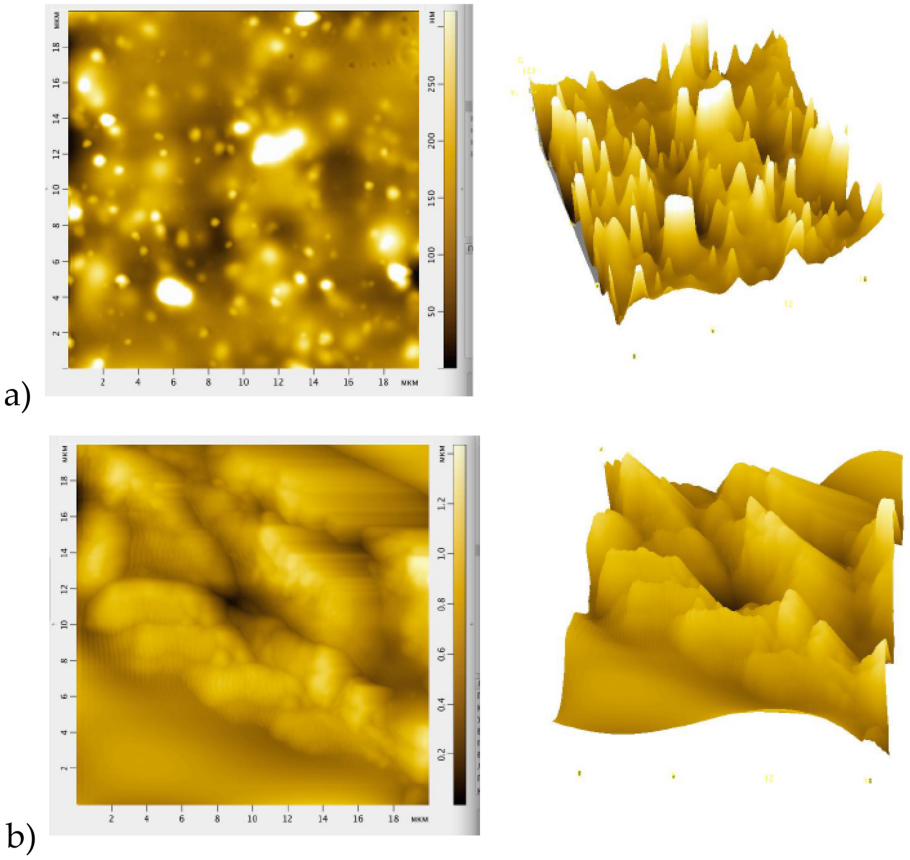

Fig. 17. AFM image of PAP/GO (a) and PAP/SWCNT (b) [13].

PEC exhibits a uniform surface without pronounced structural elements. The PEC/SWCNT composite exhibits characteristic fibrous structure corresponding to nanotubes, uneven density distribution over the sample surface. The PEC/GO system exhibits uniformly distributed structures over the surface, formation of large “island” structures [14].

The most representative SEM images of the specified carbon material at various magnifications are presented. According to the data obtained, the fibrous structure of the surface of the film of the obtained carbon material is clearly visible (Fig.19) [17].

The morphology of the carbon layer is shown in Fig. 20. The scanning electron microscopy (SEM)

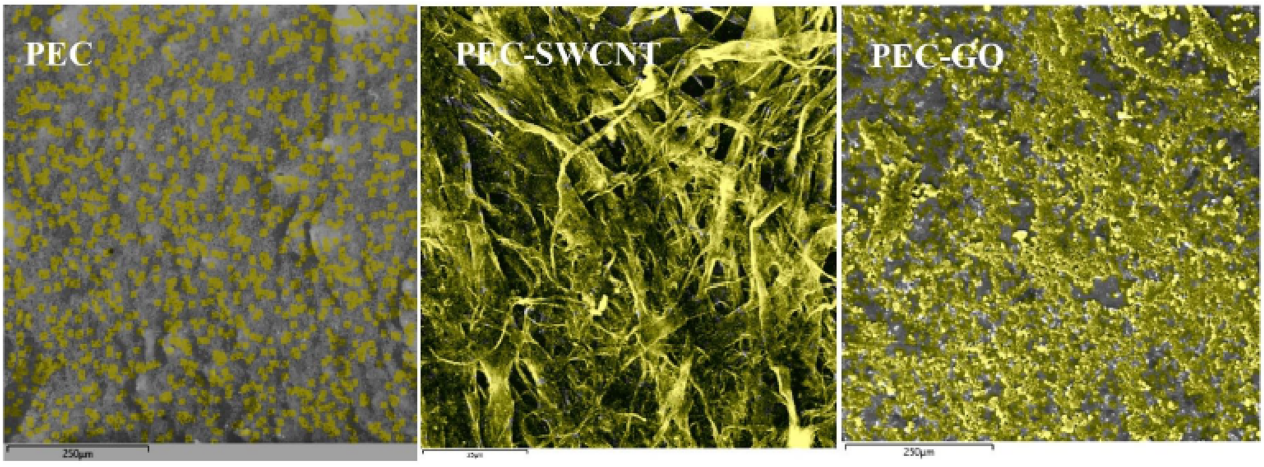

Fig. 18. SEM images of PEC (left), PEC-SWCNT (middle) and PEC-GO (right) in carbon (yellow) contrast [14].

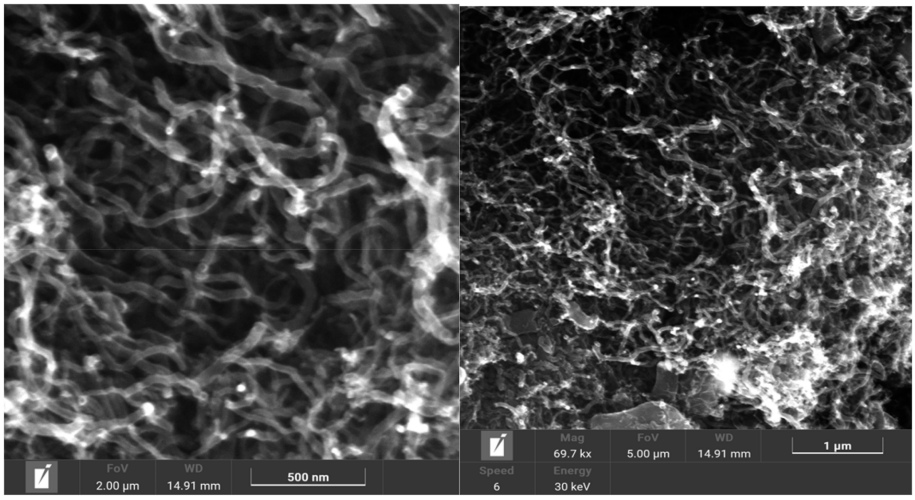

Fig. 19. SEM images of the obtained nanocarbon [17].

studies revealed the following structural features: preservation of the integrity of the CNT structure in the presence of high curvature; formation of intertwined aggregates without signs of defects; high-quality distribution over the surface, indicating an optimized deposition technology. The silicon substrate provides surface smoothness for uniform distribution and high contrast during SEM observations [61,62]. The key factor in controlling the layer morphology is the CNT deposition rate. By varying this rate, one can control the structural features of the film and the physicochemical properties of the resulting layers [18].

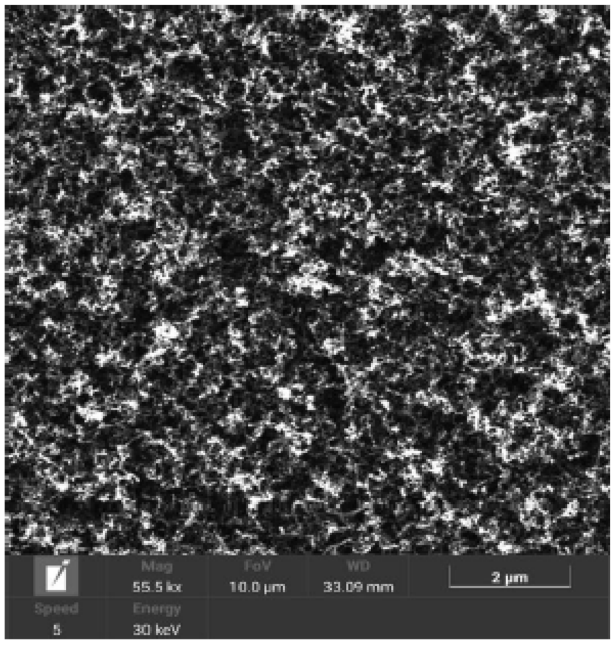

Fig. 20. SEM images of the obtained epoxy mixture of CNTs [18].

The morphology of the surfaces of the films was also studied. Atomic force microscopy (AFM) images (Fig. 21) were obtained using Nanoeducator II NT-MDT instrument, scan size = 20 by 20 µm.

4. Carrier mobility in thin-film field-effect transistors

Charge carrier mobility (µ) is a key parameter characterizing the performance of thin-film field-effect transistors. Improvement of mobility is achieved by optimizing the morphology of the active layer, using highly ordered molecules and introducing nanocomposite additives that help increase the degree of crystallinity and reduce defects.

Homogeneous and ordered structures with low surface roughness values usually lead to increased charge carrier mobility [21].

The mobility of charge carriers is given by:

$$\mu = \frac{I_{DS}}{\frac{W}{L}\cdot C\cdot\left(V_G - V_{th} - \frac{V_{DS}}{2}\right)\cdot V_{DS}}, \quad (1)$$

where W is the channel width, L is the channel length, C is the capacitance per square area of the gate dielectric AlO_X (for the 500 nm thickness, $C = 7.1$ nF/cm^2), V_G is the gate voltage, V_{DS} is the voltage between the drain and source, and U_{th} is the threshold voltage. The threshold voltage V_{th} is found from the plots of the current root $I_{DS}{}^{1/2}$ versus the voltage V_{DS} at V_G = const.

The calculated values of the charge carriers' mobility for different kinds of OFETs are shown in Table 1.

As can be seen from Table 1, the value of charge carrier mobility in thin film samples of field-effect transistors depends on the material. Traditional polymers (P3HT) show modest results (0.0073 cm^2/V s)

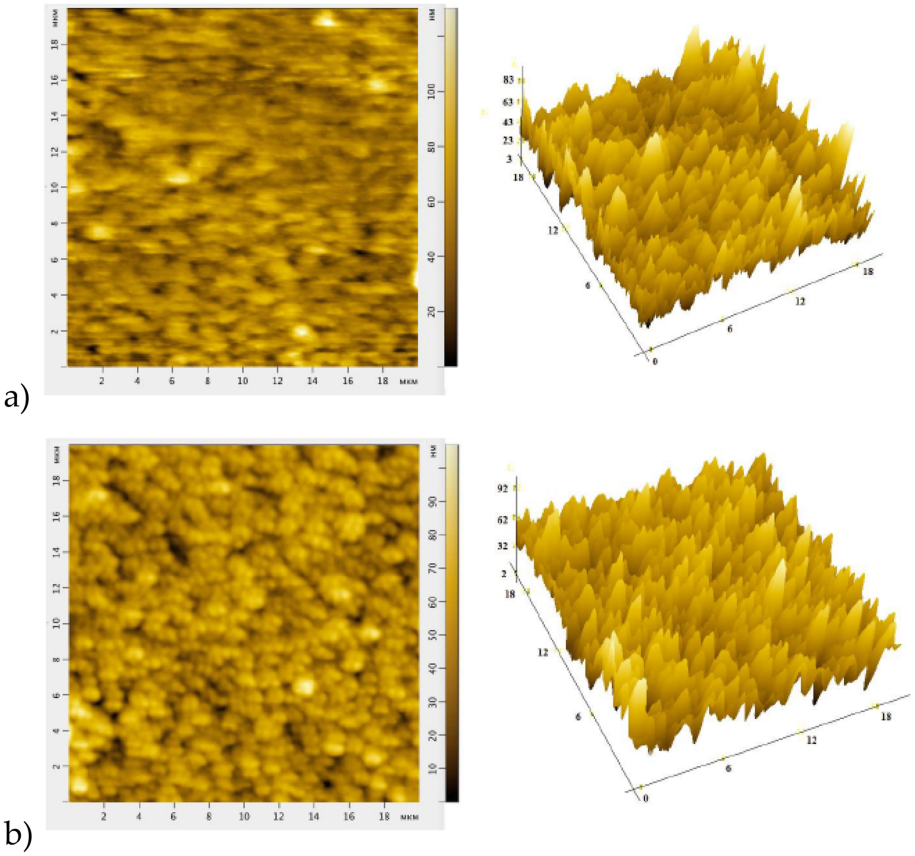

*Fig. 21. AFM image of the film formed from compound (a) **4** and (b) **6** [51].*

Table 1. Comparison of charge carriers' mobility for different kinds of thin films.

Sample*	Mobility, $cm^2/V \cdot s$
CNTN [7].	1
P3HT-based M-OTFT [8].	0.0073
PAP/GO	0.020
PAP/SWCNT [13].	0.071
PEC	0.34
PEC/GO	0.97
PEC/CP	0.96
PEC/CB	0.57
PEC/SWCNT	1.12
PEC/GO + SWCNT [14].	10.97
SCTS	0.173
SCTS-GO	0.509
SCTS-CP	0.351
SCTS-CB	0.269
SCTS-SWCNT [15].	0.713
Nano-S [17].	0.008
CNT-Epoxy [18].	28.87
CNTs in a polyarylene phthalide matrix [21].	0.007
2-naphthyl molecules	0.09
biphenyl-4-yl molecules [51].	0.033
pgBTTT [63].	3.440
P(bgDPP-MeOT2) [64].	1.630
p(gDPP-T2) [65].	1.550

(*continued on next page*)

Table 1. (continued)

Sample*	Mobility, $cm^2/V \cdot s$
PProDOT-DPP [66].	0.940
P3gCPDT-1gT2 [67].	0.900
pFBT with chalcogenoselenophene [68].	0.250
f-BTI2g-TVTCN [69].	0.240

*CNTN: Carbon Nanotube Network [7].
P3HT-based M-OTFT: Poly(3-hexylthiophene-2,5-diyl)-based Modified Organic Thin-Film Transistor [8].
PAP/GO: Polyarylenephthalide/Graphene Oxide composite [13].
PAP/SWCNT: Polyarylenephthalide/Single-Walled Carbon Nanotube composite [13].
PEC: Polyelectrolyte Complex (based on chitosan and chitosan succinate) [14].
PEC/GO: Polyelectrolyte Complex/Graphene Oxide composite [14].
PEC/CP: Polyelectrolyte Complex/Carbopack composite [14].
PEC/CB: Polyelectrolyte Complex/Carbon Black (Carboblack C) composite [14].
PEC/SWCNT: Polyelectrolyte Complex/Single-Walled Carbon Nanotube composite [14].
PEC/GO + SWCNT: Polyelectrolyte Complex/Graphene Oxide + Single-Walled Carbon Nanotube hybrid composite [14].
SCTS: Succinyl Chitosan [15].
SCTS-GO: Succinyl Chitosan/Graphene Oxide composite [15].
SCTS-CP: Succinyl Chitosan/Carbopack composite [15].
SCTS-CB: Succinyl Chitosan/Carbon Black composite [15].
SCTS-SWCNT: Succinyl Chitosan/Single-Walled Carbon Nanotube composite [15].
Nano-S: Nanofibrous Carbon [17].
CNT-Epoxy: Carbon Nanotube/Epoxy resin composite [18].
CNTs in a polyarylene phthalide matrix: Carbon Nanotubes in a Polyarylenephthalide matrix [21].
2-naphthyl molecules: 1-(4-(2-naphthyl)-1,2,3-triazol-1-yl)-2-butylfullerene derivative [51].
biphenyl-4-yl molecules: 1-(4-(biphenyl-4-yl)-1,2,3-triazol-1-yl)-2-butylfullerene derivative [51].
pgBTTT: Poly(germyl-bis-thienothiophene) [63].
P(bgDPP-MeOT2): Polymer based on benzodithiophene and diketopyrrolopyrrole with methyloxy-thiophene side chains [64].
p(gDPP-T2): Polymer based on diketopyrrolopyrrole and bithiophene [65].
PProDOT-DPP: Poly(propylenedioxythiophene-diketopyrrolopyrrole) [66].
P3gCPDT-1gT2: Polymer based on cyclopentadithiophene and bithiophene [67].
pFBT with chalcogenoselenophene: Poly(fullerothiophene) with chalcogenoselenophene comonomer [68].
f-BTI2g-TVTCN: Fluorinated bithienoindacenodithiophene-based polymer with TVTCN group [69].

[8]. The highest mobility is demonstrated by CNT-Epoxy (28.87 cm^2/V s) and PEC/GO + SWCNT (10.97 cm^2/V s) composites, which confirms the efficiency of using carbon nanomaterials as fillers [14,18]. The addition of GO and SWCNT to polymer matrices (PEC, SCTS) increases the mobility by 2−60 times compared to pure polymers [13−15]. New derivatives (biphenyl-4-yl and 2-naphthyl molecules) demonstrate intermediate values (0.033−0.09 cm^2/V s) [51]. High pgBTTT values (3.44 cm^2/V s) and other polymers [63−65] indicate the potential of molecular design of organic semiconductors.

Above, we discussed modern achievements in the development of such transistors based on organic and nanocomposite materials, including carbon nanotubes, graphene oxide and polymers. Analysis of their electrical properties, charge carrier mobility and surface morphology confirms the potential for use in flexible electronics, sensors and biomedical devices [70−78].

5. Conclusions

This review examined recent progress in developing organic field-effect transistors (OFETs) based on a range of materials, including carbon nanotubes, graphene oxide, poly(3-hexylthiophene-2,5-diyl) (P3HT), polyarylenephthalide (PAP) composites, and fullerene derivatives. A key finding was that the performance of these devices is intrinsically linked to the morphology and composition of the active layer. Microscopy and electrical characterization confirmed that incorporating nanofillers like single-walled carbon nanotubes (SWCNTs) and graphene oxide (GO) into polymer matrices enhanced crystallinity, reduced structural defects, and consequently improved charge carrier mobility.

However, several challenges persist. Non-ideal output characteristics, including a lack of current saturation, were frequently observed and often attributed to leakage currents or suboptimal film morphology. The research surveyed indicated that the primary hurdles for widespread adoption remain enhancing environmental stability, achieving lower operating voltages, and ensuring high reproducibility.

Future efforts should prioritize optimizing deposition techniques, designing novel composite materials, and refining device architectures. Addressing these areas is essential for advancing this technology from laboratory research to practical applications in sensing, wearable systems, and large-area electronics.

Funding

The research was funded with the support of the Russian Federation state assignment (scientific code FZWU-2023-0002).

Conflicts of interest

The authors declare that they have no known competing financial interests or personal relationships that could have appeared to influence the work reported in this paper.

References

[1] Y. Fan, J. Liu, W. Hu, Y. Liu, L. Jiang, J. Mater. 8 (2020) 13154.
[2] Y.J. Wang, Q. Gong, Q. Miao, Mater. Chem. Front. 4 (2020) 3505.
[3] S. Yuvaraja, A. Nawaz, Q. Liu, D. Dubal, S.G. Surya, K.N. Salama, P. Sonar, Chem. Soc. Rev. 49 (2020) 3423.
[4] H. Dong, X. Fu, J. Liu, Z. Wang, W. Hu, Adv. Mater. 25 (2013) 6188.
[5] Y. Zang, D. Huang, C.A. Di, D. Zhu, Adv. Mater. 28 (2016) 4549.
[6] H. Li, W. Shi, J. Song, H.J. Jang, J. Dailey, J. Yu, H.E. Katz, Chem. Rev. 119 (2019) 3.
[7] M.Y. Zavodchikova, T. Kulmala, A.G. Nasibulin, V. Ermolov, S. Franssila, K. Grigoras, E.I. Kauppinen, Nanotechnology 20 (8) (2009) 085201.
[8] E.N. Tarekegn, M. Seyedi, I. Luzinov, W.R. Harrell, Polymers 14 (2022) 5061.
[9] M. Małachowski, J. Żmija, Opto-Electron. Rev. 18 (2) (2010) 121−136.
[10] A. Bunakov, A. Lachinov, R. Salikhov, Macromol Symp 212 (1) (2004) 387−392.
[11] R.B. Salikhov, A.N. Lachinov, A.A. Bunakov, Phys Solid State 49 (2007) 185−188.
[12] A.G. Mustafin, L.R. Latypova, A.N. Andriianova, S.M. Salikhov, A. F. Sattarova, I.N. Mullagaliev, I.B. Abdrakhmanov, Macromolecules 53 (18) (2020) 8050−8059.
[13] R.B. Salikhov, R.A. Zilberg, I.N. Mullagaliev, T.R. Salikhov, Y. B. Teres, Mendeleev Commun 32 (2022) 520−522.
[14] R.A. Zilberg, R.B. Salikhov, I.N. Mullagaliev, T.R. Salikhov, Y. B. Teres, E.O. Bulysheva, A.D. Ostaltsova, Chimica. Techno. Acta 11 (3) (2024) 202411302.
[15] R. Salikhov, R. Zilberg, I. Mullagaliev, T. Salikhov, Y. Teres, E. Bulysheva, A. Ostaltsova, Current Nanomed. 15 (1) (2025) 70−79.
[16] K. Liu, T. Duan, F. Zhang, X. Tian, H. Li, M. Feng, K. Zhang, J Mater Chem 12 (32) (2024) 20606−20637.
[17] I.A. Mustafin, A.F. Akhmetov, R.B. Salikhov, I.N. Mullagaliev, T. R. Salikhov, R.N. Galiakhmetov, A.G. Mustafin, Chimica. Techno. Acta 11 (4) (2024) 202411421.
[18] T. Yumalin, T. Salikhov, B. Mahato, A. Shiverskii, S. Abaimov, R. Salikhov, Chimica. Techno. Acta 11 (2) (2024) 202411205.
[19] P. Li, Y. Zhang, Z. Zheng, Adv Mater 31 (2019) 1902987.
[20] A.N. Andriianova, R.B. Salikhov, L.R. Latypova, I.N. Mullagaliev, T.R. Salikhov, A.G. Mustafin, Sustain. Energy Fuels 6 (2022) 3435−3445.
[21] A.R. Tuktarov, R.B. Salikhov, A.A. Khuzin, I.N. Safargalin, I. N. Mullagaliev, O.V. Venidiktova, U.M. Dzhemilev, Mendeleev Commun 29 (2019) 160−162.
[22] A. Bunakov, A. Lachinov, R. Salikhov, Macromol Symp 212 (2004) 387−392.
[23] G. Collins, P. Avouris, Sci Am 283 (2000) 62−69.
[24] X. Zhang, W. Lu, G. Zhou, Q. Li, Adv. Mater. 32 (2020) 1902028.
[25] M. Kavitha, A.M. Kalpana, I-manager's J. Electron. Eng. 7 (3) (2017) 1.
[26] H.E. Katz, Chem. Mater. 16 (23) (2004) 4748−4756.
[27] P.L. McEuen, M.S. Fuhrer, H. Park, IEEE Trans. Nanotechnol. 1 (1) (2002) 78−85.
[28] D.-M. Sun, M.Y. Timmermans, Y. Tian, A.G. Nasibulin, E. I. Kauppinen, S. Kishimoto, T. Mizutani, Y. Ohno, Nat. Nanotechnol. 6 (3) (2011) 156−161.
[29] S.W. Lee, S.Y. Lee, S.C. Lim, Y.-D. Kwon, J.-S. Yoon, K. Uh, Y. H. Lee, Appl. Phys. Lett. 101 (5) (2012) 053504.
[30] H. Jung, S. Choi, J.T. Jang, J. Yoon, J. Lee, Y. Lee, J. Rhee, G. Ahn, H. R. Yu, D.M. Kim, S.-J. Choi, D.H. Kim, Solid State Electron. 140 (2018) 80−85.
[31] S. Pyo, J. Choi, J. Kim, Adv. Electron. Mater. 5 (2) (2019) 1800737.
[32] S.W. Lee, D. Suh, S.Y. Lee, Y.H. Lee, Appl. Phys. Lett. 104 (16) (2014) 163506.
[33] H. Ni, M. Li, X. Li, X. Zhu, H. Liu, M. Xu, L. Wang, S. Qiu, J. Peng, IEEE Trans. Electron Dev. 69 (3) (2022) 1069−1076.
[34] F.M. Albarghouthi, N.X. Williams, J.L. Doherty, S. Lu, A. D, ACS Appl. Nano Mater. 5 (10) (2022) 15865−15874.
[35] H. Yoo, J. Ha, H. Kim, J. Seo, S.-Y. Lee, Y. Hong, IEEE Electron Device Lett. 41 (6) (2020) 860−863.
[36] M. Yu, H. Wan, L. Cai, J. Miao, S. Zhang, C. Wang, ACS Nano 12 (11) (2018) 11572−11578.
[37] J. Ha, H. Yoo, J. Seo, Y. Hong, ACS Appl. Mater. Interfaces 15 (2) (2023) 3192−3201, 2023.
[38] S. Kim, S. Kim, J. Park, S. Ju, S. Mohammadi, ACS Nano 4 (6) (2010) 2994−2998.
[39] E.S. Snow, J.P. Novak, P.M. Campbell, D. Park, Appl. Phys. Lett. 82 (13) (2003) 2145−2147.
[40] L. Hu, D.S. Hecht, G. Gruner, Nano Lett. 4 (12) (2004) 2513−2517.
[41] C. Kocabas, N. Pimparkar, O. Yesilyurt, S.J. Kang, M.A. Alam, J. A. Rogers, Nano Lett 7 (5) (2007) 1195−1202.
[42] W. Kim, A. Javey, O. Vermesh, Q. Wang, Y. Li, H. Dai, Nano Lett 3 (2) (2003) 193−198.
[43] D.B. Farmer, R.G. Gordon, Nano Lett 6 (4) (2006) 699−703.
[44] A. Javey, J. Guo, D.B. Farmer, Q. Wang, E. Yenilmez, R.G. Gordon, H. Dai, Nano Lett 4 (7) (2004) 1319−1322.
[45] E.S. Snow, P.M. Campbell, M.G. Ancona, J.P. Novak, Appl. Phys. Lett. 86 (3) (2005) 033105.
[46] N. Pimparkar, Q. Cao, S. Kumar, J.Y. Murthy, J. Rogers, M. A. Alam, IEEE Electron Device Lett. 28 (2) (2007) 157−159.
[47] S.K. Kim, Y. Xuan, P.D. Ye, S. Mohammadi, J.H. Baek, M. Shim, Appl. Phys. Lett. 90 (16) (2007) 163108.
[48] A.A. Akhmetov, R.I. Aminov, I.N. Mullagaliev, R.B. Salikhov, Russ. J. Gen. Chem. 93 (9) (2023) 1315−1325.
[49] A.A. Akhmetov, R.I. Aminov, I.N. Mullagaliev, R.B. Salikhov, Russ. J. Gen. Chem. 93 (9) (2023) 2193−2201.
[50] A.R. Akhmetov, R.I. Aminov, Z.R. Sadretdinova, R.B. Salikhov, I. N. Mullagaliev, T.R. Salikhov, Curr. Org. Chem. 27 (14) (2023) 1277−1287.
[51] Z.R. Sadretdinova, A.R. Akhmetov, R.B. Salikhov, I. N. Mullagaliev, T.R. Salikhov, Mendeleev. Commun. 33 (2023) 320−322.
[52] T.G. Krinke, K. Deppert, M.N. Magnusson, F. Schmidt, H. Fissan, J. Aerosol. Sci. 33 (2002) 1341.
[53] E.N. Tarekegn, W.R. Harrell, I. Luzinov, W. Delaney, ECS J. Solid State Sci. Technol. 11 (2022) 025008.
[54] S.H. Kim, I. Kang, Y.G. Kim, H.R. Hwang, Y.H. Kim, S.K. Kwon, J. Jang, J. Mater Chem 1 (13) (2013) 2408−2411.
[55] C. Avis, H.R. Hwang, J. Jang, ACS Appl. Mater. Interfaces 6 (14) (2014) 10941−10945.
[56] Z.R. Sadretdinova, A.R. Akhmetov, A.R. Tulyabaev, Yu. H. Budnikova, Yu.B. Dudkina, A.R. Tuktarov, U.M. Dzhemilev, Org. Biomol. Chem. 19 (2021) 9299.
[57] A.G. Nasibulin, A. Moisala, D.P. Brown, H. Jiang, Chem. Phys. Lett. 402 (2005) 227.
[58] C.R. Singh, G. Gupta, R. Lohwasser, S. Engmann, J. Balko, M. Thelakkat, T. Thurn-Albrecht, H. Hoppe, J. Polym. Sci. Part B Polym. Phys. 51 (2013) 943−951.
[59] H. Yang, T.J. Shin, L. Yang, K. Cho, C.Y. Ryu, Z. Bao, Adv. Funct. Mater. 15 (2005) 671−676.
[60] R.J. Kline, M.D. McGehee, E.N. Kadnikova, J. Liu, J.M. Fréchet, Adv. Mater. 15 (2003) 1519−1522.

[61] S. Sandoval, M. Kierkowicz, E. Pach, B. Ballesteros, G. Tobias, MethodsX 5 (2018) 1465−1472.
[62] X. Huang, R. Farra, R. Schlögl, M.G. Willinger, Nano Lett. 19 (8) (2019) 5380−5387.
[63] R.K. Hallani, B.D. Paulsen, A.J. Petty, J. Am. Chem. Soc. 143 (2021) 11007−11018.
[64] H. Jia, Z. Huang, P. Li, S. Zhang, Y. Wang, J.-Y. Wang, X. Gu, T. Lei, J. Mater. Chem. C 9 (2021) 4927−4934.
[65] M. Moser, A. Savva, K. Thorley, B.D. Paulsen, T.C. Hidalgo, D. Ohayon, H. Chen, A. Giovannitti, A. Marks, N. Gasparini, A. Wadsworth, J. Rivnay, S. Inal, I. McCulloch, Angew. Chem. Int. Ed. 60 (2021) 7777−7785.
[66] X. Luo, H. Shen, K. Perera, D.T. Tran, B.W. Boudouris, J. Mei, ACS Macro. Lett. 10 (2021) 1061−1067.
[67] L. Lan, J. Chen, Y. Wang, P. Li, Y. Yu, G. Zhu, Z. Li, T. Lei, W. Yue, I. McCulloch, Chem. Mater. 34 (2022) 1666−1676.
[68] M. Sung, H. Yoo, D. Yoo, M. Deligios, E. Taviani, S.E. Simbine, T. Zimba, J. Sacarlal, S. Rubino, B. Paglietti, Org. Electron. 111 (2022) 106649.
[69] K. Feng, W. Shan, J. Wang, J.-W. Lee, W. Yang, W. Wu, Y. Wang, B. J. Kim, X. Guo, H. Guo, Adv. Mater. 34 (2022) 2201340.
[70] P.R. Bandaru, J. Nanosci. Nanotechnol. 7 (4−5) (2007) 1239−1267.
[71] W. Bauhofer, J.Z. Kovacs, Compos. Sci. Technol. 69 (10) (2009) 1486−1498.
[72] A.G. Mustafin, L.R. Latypova, A.N. Andriianova, I.N. Mullagaliev, S.M. Salikhov, R.B. Salikhov, G.S. Usmanova, RSC Adv. 11 (34) (2021) 21006−21016.
[73] A.N. Andriianova, R.B. Salikhov, L.R. Latypova, I.N. Mullagaliev, T.R. Salikhov, A.G. Mustafin, Sustain. Energy Fuels 6 (14) (2022) 3435−3445.
[74] R.B. Salikhov, I.N. Mullagaliev, B.R. Badretdinov, A.D. Ostaltsova, T.T. Sadykov, A.G. Mustafin, Lett. Mat. 12 (4) (2022) 309−315.
[75] R.B. Salikhov, A.D. Ostaltsova, T.R. Salikhov, Bull. Russ. Acad. Sci. Phys. 89 (3) (2025) 386−390.
[76] R.B. Salikhov, A.D. Ostaltsova, T.R. Salikhov, Kh.M. Balapanov, E.S. Bugybayev, Eurasian J. Phys. Func. Mat. 8 (2) (2024) 58−70.
[77] R.B. Salikhov, R.A. Zilberg, E.O. Bulysheva, A.D. Ostaltsova, T. R. Salikhov, Y.B. Teres, Letters Mat. 13 (2) (2023) 132−137.
[78] R.B. Salikhov, A.D. Ostaltsova, T.R. Salikhov, Kh.M. Balapanov, M.M. Kubenova, Eurasian J. Phys. Func. Mat. 9 (1) (2025) 1−10.